

# Catalysis Science & Technology

Accepted Manuscript



This is an *Accepted Manuscript*, which has been through the Royal Society of Chemistry peer review process and has been accepted for publication.

*Accepted Manuscripts* are published online shortly after acceptance, before technical editing, formatting and proof reading. Using this free service, authors can make their results available to the community, in citable form, before we publish the edited article. We will replace this *Accepted Manuscript* with the edited and formatted *Advance Article* as soon as it is available.

You can find more information about *Accepted Manuscripts* in the [Information for Authors](#).

Please note that technical editing may introduce minor changes to the text and/or graphics, which may alter content. The journal's standard [Terms & Conditions](#) and the [Ethical guidelines](#) still apply. In no event shall the Royal Society of Chemistry be held responsible for any errors or omissions in this *Accepted Manuscript* or any consequences arising from the use of any information it contains.

## **Copper nanoparticles decorated polyaniline-zeolite nanocomposite for the nanomolar simultaneous detection of hydrazine and phenylhydrazine**

Balwinder Kaur<sup>a</sup>, Rajendra Srivastava\*<sup>a</sup>, and Biswarup Satpati<sup>b</sup>

*<sup>a</sup>Department of Chemistry, Indian Institute of Technology Ropar, Rupnagar-140001, India*

*<sup>b</sup>Surface Physics and Material Science Division, Saha Institute of Nuclear Physics, 1/AF, Bidhannagar, Kolkata 700 064, India*

---

E-mail: rajendra@iitrpr.ac.in

Phone: +91-1881-242175; Fax: +91-1881-223395

---

**Abstract**

In this work, highly dispersed copper nanoparticles decorated polyaniline-nanocrystalline zeolite organic-inorganic hybrid material was synthesized. Hybrid material was characterized by the complementary combination of X-ray diffraction, N<sub>2</sub>-adsorption, scanning-transmission electron microscopy, Fourier transform infrared spectroscopy, and thermo gravimetric techniques. An electrochemical sensor based on copper nanoparticles supported polyaniline-nanocrystalline zeolite was developed for the nanomolar simultaneous detection of environmental pollutants hydrazine and phenylhydrazine with high electrocatalytic activity, stability, sensitivity, and selectivity. Under the optimum condition, a wide linear range was obtained from 4 nM-800 μM with a limit of detection of 1 nM for both hydrazine and phenylhydrazine. The analytical performance of the developed sensor was demonstrated for the determination of hydrazine and phenylhydrazine in different water bodies with satisfactory results.

**Keywords:** Copper nanoparticles; Nanocrystalline zeolite; Polyaniline; Electrocatalytic oxidation; Simultaneous determination; Hydrazine; Phenylhydrazine

---

## 1. Introduction

Human activity such as agricultural and industrial revolution (to cater the need of large population) largely contributes to the contamination of the environment that imbalance the ecosystem. Among various toxic pollutants, hydrazine (HZ) and its derivative (such as phenylhydrazine (PhZ)) are widely used as agricultural pesticides, pharmaceutical intermediates, explosives, photography chemicals, corrosive inhibitors, rocket propellants, and fuel cells.<sup>1-4</sup> HZ and PhZ are neurotoxin, carcinogenic, and corrosive in nature.<sup>5</sup> HZ and PhZ poisoning, even at lower concentration, may cause vomiting, skin irritation, dermatitis, hemolytic anemia, severe irritation to the respiratory tract, adverse effect on the liver and kidney, and long term effect on central nervous system.<sup>3, 6, 7</sup> HZ and PhZ exhibit carcinogenic risk to human health and they are classified in group B2 by the World Health Organization and Environmental Protection Agency.<sup>8, 9</sup> Therefore, detection of trace amount of HZ and PhZ is of significant importance. Several analytical methods are known for the detection of HZ and PhZ.<sup>10-15</sup> Among these, electroanalytical techniques provide direct and efficient detection of these environmental pollutants. However, electroanalytical methods using conventional electrodes exhibit low sensitivity, poor reproducibility, slow electron transfer kinetics and require high overpotential for the oxidation of HZ and PhZ.<sup>4</sup> To overcome these problems associated with conventional electrodes, chemically modified electrodes are being developed that contain selected redox mediators immobilized on conventional electrodes.<sup>16-19</sup> In the recent years, noble metal nanoparticles, especially gold, palladium, and silver have been investigated in the HZ sensing with good electrochemical activity.<sup>20-22</sup> However, expensive materials limit its practical applications. Alternatively, non noble metal catalysts such as transition metal oxides ( $\text{Fe}_2\text{O}_3$ ,  $\text{WO}_3$ ,  $\text{MnO}_2$ ,  $\text{CuO}$ ,  $\text{ZnO}$ ), transition metal complexes, metal oxide-graphene composites, and carbon nanotubes have been explored as electrode materials for the detection of HZ and PhZ.<sup>4, 23-27</sup> However, lengthy procedure and higher limit of detection are some of the drawbacks of these electrodes. Therefore, it is highly desirable to develop economical electrodes for the sensitive determination of HZ and PhZ. Although a number of reports are available in the literature for HZ detection but only a few reports are known for PhZ.<sup>1, 3, 4, 19, 26, 28-31</sup> Moreover, the simultaneous determination of HZ and PhZ is rarely reported.<sup>5</sup> Therefore, an efficient and robust approach is required for the simultaneous determination of HZ and PhZ, with low limit of detection. The present manuscript focuses to achieve this objective.

Our research is mainly focused on the development of nanocomposite materials based on mesoporous zeolites, polyaniline, metal oxides and find their application in the fabrication of efficient electrochemical sensors.<sup>32-41</sup> In the recent years, application of nanocrystalline zeolites based chemically modified electrodes for the electrochemical detection of important biomolecules and organic/inorganic water pollutants has been demonstrated.<sup>32-35, 37, 39</sup> Nanocomposite materials enhance the electrocatalytic performance since they combine the advantage features associated with its constituents. We have recently shown the high electroactivity of polyaniline-zeolite nanocomposite material when compared to polyaniline or nanocrystalline zeolite.<sup>41</sup> The incorporation of redox active centre in polyaniline-zeolite nanocomposite further enhanced the electrocatalytic activity.<sup>41</sup>

In this study, we present the synthesis of highly dispersed copper nanoparticles decorated nanoporous polyaniline-zeolite (CuNPs-PANI-Nano-ZSM-5) nanocomposite material and find their application as electrochemical sensor for the sensitive and simultaneous detection of HZ and PhZ. CuNPs-PANI-Nano-ZSM-5 based sensor exhibited remarkably high activity and sensitivity when compared to its individual constituent's, PANI and Nano-ZSM-5. The results demonstrate that CuNPs-PANI-Nano-ZSM-5 nanocomposite has potential to act as a promising electrode material for the simultaneous detection of HZ and PhZ.

## 2. Experimental Section

### 2.1. Materials

All chemicals were of AR grade and used as received without further purification. Tetraethylorthosilicate (TEOS, 98%), tetrapropylammonium hydroxide (TPAOH), propyltriethoxy silane (PrTES, 97%), 3-aminopropyl trimethoxysilane, and poly(ethylene glycol)-block-poly(propylene glycol)-block-poly(ethylene glycol) (EO<sub>20</sub>PO<sub>70</sub>EO<sub>20</sub>, MW 5800) (hereafter designated as P123) were purchased from Sigma Aldrich, India. Aniline, ammonium peroxydisulphate (APS), and sodium borohydride were obtained from Spectrochem Pvt. Ltd., India. Copper nitrate trihydrate (CuNO<sub>3</sub>.3H<sub>2</sub>O) was obtained from Loba Chemie Pvt. Ltd., India. Sodium dodecyl sulfate was obtained from S D Fine Chemical Ltd., India. Deionized water from Millipore Milli-Q system (Resistivity 18 MΩcm) was used in the electrochemical studies. Electrochemical measurements were performed in 0.1 M phosphate buffer (*Sorenson's buffer*)

solution, which was prepared by mixing  $\text{NaH}_2\text{PO}_4$  and  $\text{Na}_2\text{HPO}_4$ . The standard phosphate buffer solutions (PBS) with different pH values (lower or higher) were prepared by adding 0.1 M aqueous  $\text{H}_3\text{PO}_4$  or NaOH solution to 0.1 M aqueous PBS, while magnetically stirring until the pH of the aqueous solution reached the desired value. All electrochemical experiments were performed in 0.1 M PBS at pH 8.5, unless specified otherwise.

## 2.2. Synthesis of CuNPs decorated PANI-Nano-ZSM-5 nanocomposite

Nanocrystalline ZSM-5 zeolite (Nano-ZSM-5) was prepared using molar composition TEOS/10 PrTES/2.5  $\text{Al}_2\text{O}_3$ /3.3  $\text{Na}_2\text{O}$ /25 TPAOH/2500  $\text{H}_2\text{O}$  by following the reported procedure.<sup>32</sup> Propyl amine was then covalently anchored on the external surface of Nano-ZSM-5. Nano-ZSM-5 (2 g) and (3-aminopropyl)trimethoxysilane (1.43 g) were taken in 50 mL toluene and the reaction mixture was refluxed for 12 h. After the reaction, the reaction mixture was filtered and solid sample was washed with toluene followed by acetone and dried at 323 K for 24 h in oven to obtain propyl amine-functionalized Nano-ZSM-5 (hereafter represented as Nano-ZSM-5-Pr-NH<sub>2</sub>).

In a typical synthesis of PANI-Nano-ZSM-5 nanocomposite, first P123 (0.150 g) was dispersed in 600 mL deionized water. Then 0.5 g of Nano-ZSM-5-Pr-NH<sub>2</sub> was added to this mixture, followed by the addition of sodium dodecyl sulfate (0.312 g). The mixture was then ultrasonically dispersed for 15 min. A solution of aniline (0.5 g) and HCl (10 mL, 1 M) was added drop wise to the above mixture with vigorous stirring. The mixture was then kept in cold water bath (~ 290 K) and mechanically stirred for 30 minutes. An ice cold aqueous solution of APS (2.45 g of APS in 10 mL of deionized water) was added into the above mixture instantly to start the oxidative polymerization and the reaction was allowed to proceed for 5 h under mechanical stirring. After the reaction, the resulting precipitate was washed with 0.1 M ammonium acetate followed by deionized water and ethanol, several times. The final product was dried in vacuum at 333 K for 12 h to obtain the PANI-Nano-ZSM-5 nanocomposite. For comparison, conventional PANI was prepared using the reported procedure.<sup>42</sup>

For the synthesis of copper nanoparticles decorated PANI-Nano-ZSM-5 nanocomposite (hereafter represented as CuNPs(5%)-PANI-Nano-ZSM-5),  $\text{CuNO}_3 \cdot 3\text{H}_2\text{O}$  (38 mg) was dissolved in 15 mL deionized water.  $\text{CuNO}_3$  solution was added drop wise to a 50 mL aqueous solution containing sodium dodecyl sulfate (62.3 mg) and  $\text{NaBH}_4$  (35.7 mg) at 276-277 K under magnetic

stirring. The reaction was continued for 30 min at 276-277 K with constant stirring. This resulted in the formation of a black colloidal solution due to the formation of Cu nanoparticles. In another beaker, PANI-Nano-ZSM-5 (200 mg) was dispersed in 10 mL deionized water. The dispersed PANI-Nano-ZSM-5 was then added to the colloidal Cu nanoparticles solution at ambient temperature and kept under stirring conditions for 5 h. The resulting product was centrifuged, washed with ethanol and water, followed by drying in vacuum at 333 K. CuNPs-PANI-Nano-ZSM-5 nanocomposites with different weight ratios (3, 6, and 10, denoted as CuNPs(3%)-PANI-Nano-ZSM-5, CuNPs(6%)-PANI-Nano-ZSM-5, and CuNPs(10%)-PANI-Nano-ZSM-5, respectively) were also synthesized using the similar procedure by varying the amount of  $\text{CuNO}_3$ . For comparison, copper nanoparticles supported conventional PANI (CuNPs(5%)-PANI) and copper nanoparticles supported Nano-ZSM-5 (CuNPs(5%)-Nano-ZSM-5) were also prepared using above mentioned procedure.

### 2.3. Instrumentation

X-ray diffraction (XRD) patterns were recorded in the  $2\theta$  range of  $5\text{-}80^\circ$  with a scan speed of  $2^\circ/\text{min}$  on a PANalytical X'PERT PRO diffractometer, using Cu  $K\alpha$  radiation ( $\lambda=0.1542$  nm, 40 kV, 40 mA) and a proportional counter detector. Nitrogen adsorption measurements were performed at 77 K by Quantachrome Instruments, Autosorb-IQ volumetric adsorption analyzer. Sample was out-gassed at 393 K for 3 h in the degas port of the adsorption apparatus. The specific surface area of zeolites was calculated from the adsorption data points obtained at  $P/P_0$  between 0.05-0.3 using the Brunauer-Emmett-Teller (BET) equation. The pore diameter was estimated using the Barret–Joyner–Halenda (BJH) method. Scanning electron microscopy (SEM) measurements were carried out on a JEOL JSM-6610LV to investigate the morphology of the materials. TEM investigations were carried out using FEI, Tecnai G<sup>2</sup> F30-ST microscope operated at 300 kV. High-angle annular dark field scanning transmission electron microscopy (HAADF-STEM) was used here using the same microscope, which was equipped with a scanning unit and a HAADF detector from Fischione (model 3000). The compositional analysis was performed using energy dispersive X-ray spectroscopy (EDS, EDAX Inc.) attachment on the Tecnai G<sup>2</sup> F30. The sample was dispersed in ethanol using ultrasonic bath and dispersed sample was mounted on a carbon coated Au grid, dried, and used for TEM measurement. Fourier transform infrared (FT-IR) spectra were recorded on a Bruker spectrophotometer in the region

600-4000  $\text{cm}^{-1}$  (spectral resolution = 4  $\text{cm}^{-1}$ ; number of scans = 100). Thermogravimetric analysis (TGA) was performed on a TGA/DSC 1 STAR<sup>e</sup> SYSTEM from Mettler Toledo instrument with temperature increments of 10 K/min in air stream.

#### 2.4. Electrode fabrication

Cyclic voltammetry (CV), differential pulse voltammetry (DPV), and chronoamperometry studies were performed using Potentiostat-Galvanostat BASi EPSILON, USA. A three-electrode electrochemical cell was employed with Ag/AgCl as the reference electrode (3M KCl), CuNPs-PANI-Nano-ZSM-5 mounted glassy carbon (3 mm diameter) as the working electrode and Pt foil as the counter electrode. Before modification, the glassy carbon electrode (GCE) was first polished to a mirror like surface with alumina slurry and then ultrasonicated in ethanol and deionized water for 5 min, respectively. 10  $\mu\text{L}$  aliquot of CuNPs-PANI-Nano-ZSM-5 suspension (a homogenous sonicated solution of 2 mg of CuNPs-PANI-Nano-ZSM-5 nanocomposite, 10  $\mu\text{L}$  of Nafion and 1 mL of deionized water) was placed onto the GCE surface. The electrode was dried in air leaving the material mounted onto the GC surface. For comparison, other modified glassy carbon electrodes were also fabricated in a similar way.

### 3. Results and discussion

#### 3.1. Physico-chemical characterization

Nano-ZSM-5 exhibited XRD pattern corresponding to a highly crystalline MFI framework structure with high phase purity (Fig. 1a). MFI is a three letter code suggested by the International Zeolite Association for ZSM-5 framework topology. XRD pattern of Nano-ZSM-5 is broad, confirming the nanocrystalline nature of the material. No change in the XRD pattern of Nano-ZSM-5-Pr-NH<sub>2</sub> was observed after the functionalization (Figure not shown), which confirms that the framework structure was not affected after the functionalization. Two broad diffraction peaks at  $2\theta = 20.5^\circ$  and  $25.1^\circ$  were obtained in the XRD pattern of PANI, which represent the periodicities parallel (100) and perpendicular (110) to the PANI chain, respectively (Fig. 1a). The XRD pattern of PANI-Nano-ZSM-5 exhibited the diffraction peaks corresponding to both, PANI and Nano-ZSM-5, phases (Fig. 1a). CuNPs(5%)-PANI-Nano-ZSM-5 also show diffraction peaks corresponding to PANI and Nano-ZSM-5 phases. Furthermore, the XRD pattern of CuNPs(5%)-PANI-Nano-ZSM-5 consists of three additional diffraction peaks located

at  $2\theta$ ; 43.3, 50.4, and 74.1°, which can be assigned to (111), (200), and (220) planes of the fcc structure of metallic Cu (Fig. 1a).<sup>43, 44</sup> This confirms the formation of CuNPs on PANI-Nano-ZSM-5 nanocomposite.

Textural properties of the synthesized materials were investigated using nitrogen adsorption-desorption measurements. Nano-ZSM-5 and PANI-Nano-ZSM-5 exhibited type-IV isotherm similar to that of mesoporous materials (Fig. 1b). A sharp increase in the volume of N<sub>2</sub> adsorption in the region  $0.4 < P/P_0 < 0.9$  is characteristic of the capillary condensation within the intercrystalline mesopore void spaces. The mesopores for Nano-ZSM-5 showed a pore size distribution in the range of 2–10 nm, whereas PANI-Nano-ZSM-5 showed somewhat narrow pore size distribution (3–8 nm). Textural properties of various materials investigated in this study are summarized in Table 1. The BET surface area and pore volume for PANI-Nano-ZSM-5 were found to be less when compared to Nano-ZSM-5. The decrease in the surface area indicates that PANI forms a thin coating around Nano-ZSM-5 particles. The total surface area and pore volume for conventional PANI were found to be very low when compared to Nano-ZSM-5 or PANI-Nano-ZSM-5.

FT-IR spectrum of PANI-Nano-ZSM-5 nanocomposite exhibited the characteristic peaks of both, PANI and Nano-ZSM-5, which further confirms the presence of both phases in the nanocomposite material (Details of FT-IR are provided in supporting information section, Fig. S1, ESI†). TGA confirms that PANI-Nano-ZSM-5 nanocomposite contains 40.7 wt % Nano-ZSM-5 and 43.8 wt % PANI. Nano-ZSM-5/PANI weight ratio was found to be 0.93, which was very close to their initial weight ratio (Details are provided in supporting information section, Fig. S2, ESI†).

SEM was used to investigate the morphology of materials investigated in this study. SEM image shows an irregular aggregated morphology for the conventional PANI (Fig. S3a, ESI†). Uniform spherical particles were obtained for Nano-ZSM-5 (Fig. S3b, ESI†). The SEM image of PANI-Nano-ZSM-5 was found to be similar to Nano-ZSM-5, which confirms that PANI film is formed on the surface of spherical Nano-ZSM-5 particles (Fig. S3c, ESI†). SEM image also confirmed that no separate phase for bulk PANI was observed. This provides indirect evidence that the growth of PANI occurred mainly at Nano-ZSM-5 surface, and not in the bulk of the aqueous zeolite suspension.

To obtain the in-depth information for CuNPs(5%)-PANI-Nano-ZSM-5, TEM investigation was made (Fig. 2). Fig. 2a shows low-magnification TEM image of Cu(5%)-PANI-Nano-ZSM-5. Fig. 2b shows the highly dispersed Cu nanoparticles on PANI-Nano-ZSM-5 support. The sizes of the copper nanoparticles vary between 5 - 10 nm as seen in the high magnification TEM image (Fig. 2c-d). To confirm the presence of Si, Al, O, and Cu elements in the material, EDS analysis was performed in STEM mode. EDX spectrum from the rectangular area 1 marked in high angle annular dark field (HAADF) image in Fig. 3a is plotted in Fig. 3b. The EDX spectrum indeed showing the elements present in CuNPs(5%)-PANI-Nano-ZSM-5.

PANI-Nano-ZSM-5 hybrid material was synthesized by the oxidative polymerization of aniline with ammonium peroxydisulfate (APS) in an aqueous zeolite suspension by the in-situ surface polymerization method. Nano-ZSM-5 was first surface functionalized with propyl amine groups that favor the growth of PANI film on the surface of Nano-ZSM-5 and not in the bulk solution. P123 (a neutral polymeric surfactant) is used to prepare a variety of mesostructured materials.<sup>42, 45</sup> P123 is amphiphilic and non ionic surfactant that can form polymer coils in aqueous solution under a dilute concentration.<sup>46</sup> P123 macromolecules could be attached to the peripheral amine groups of Nano-ZSM-5 nanoparticles through hydrogen bonding. Sodium dodecyl sulfate (SDS) was subsequently added to the solution, which could form a double surfactant layer with negative polar head group of SDS molecule. Aniline monomers could form cationic anilinium ions ( $An^+$ ) under acidic condition.  $An^+$  could adsorb on the surface of Nano-ZSM-5 with electrostatic interaction with double surfactant layer. Upon the addition of APS, PANI nucleation could take place that is stabilized by the P123/SDS double surfactant layer attached to Nano-ZSM-5 surface.<sup>47</sup> Polymerization usually takes place preferentially and continuously in proximity to existing PANI. Hence, the polymerization was initiated, propagated, and terminated on the surface of Nano-ZSM-5, rather than in bulk solution. Therefore, PANI film was formed on the surface of Nano-ZSM-5.

### 3.2. Electrochemical characteristics of modified electrode

The electrochemical behavior of CuNPs(5%)-PANI-Nano-ZSM-5/GCE was investigated using CV in 0.1 M PBS (pH 8.5) at a scan rate of 50 mV/s. CV of CuNPs(5%)-PANI-Nano-ZSM-5/GCE exhibited six peaks, which matches well with the reported literature on the bare Cu electrode (Fig. 4).<sup>32, 48, 49</sup> These redox peaks correspond to various redox couples for copper. The

oxidation peaks; peak (i), peak (ii), and peak (iii) are attributed to the Cu(0)/Cu(I), Cu(I)/Cu(II), and Cu(II)/Cu(III) redox couples, respectively.<sup>32, 48, 49</sup> The reduction peaks; peak (iv), peak (v), and peak (vi) are attributed to the Cu(III)/Cu(II), Cu(II)/Cu(I), and Cu(I)/Cu(0) redox couples, respectively (Fig. 4).

The electrochemical behavior of various modified electrodes (CuNPs(5%)-PANI-Nano-ZSM-5/GCE, PANI-Nano-ZSM-5/GCE, PANI/GCE, Nano-ZSM-5/GCE) and bare GCE was investigated using potassium ferricyanide as an electrochemical probe by CV. Study was performed in 0.1 M KCl solution containing 1 mM  $K_3[Fe(CN)_6]/K_4[Fe(CN)_6]$  at a scan rate of 10 mV/s at different modified electrodes. CV of various modified electrodes and bare GCE exhibited a pair of redox peaks corresponding to  $Fe(CN)_6^{3-/4-}$  redox couple (Fig. S4, ESI†). Fig. S4, ESI† shows that all the modified electrodes exhibited higher peak current when compared to bare GCE. This may be correlated to the porous nature of materials, which enhances the diffusion of the redox couple towards the electrode surface from the bulk.

### 3.3. Voltammetric studies of HZ and PhZ

The electrochemical behavior of HZ and PhZ was investigated in detail at CuNPs(5%)-PANI-Nano-ZSM-5/GCE. Fig. 5 shows a comparison of CVs for HZ and PhZ, individually, at CuNPs(5%)-PANI-Nano-ZSM-5/GCE and bare GCE in 0.1 M PBS (pH 8.5) at a scan rate of 50 mV/s. CV result shows well defined and sharp oxidation peaks for HZ and PhZ at CuNPs(5%)-PANI-Nano-ZSM-5/GCE (Fig. 5). However, bare GCE exhibited ill-defined voltammetric oxidation peaks for HZ and PhZ with very low peak current response and at higher oxidation potential. The oxidation peak current was 10.8 and 7.5 times higher for HZ and PhZ, respectively, at CuNPs(5%)-PANI-Nano-ZSM-5/GCE when compared to bare GCE. The poor voltammetric response at bare GCE may be attributed to the sluggish electron transfer kinetics. These results clearly show that the modification of GCE with CuNPs(5%)-PANI-Nano-ZSM-5 nanocomposite effectively accelerated the rate of electron transfer between the analytes and electrode. Based on the results obtained, it can be concluded that CuNPs(5%)-PANI-Nano-ZSM-5/GCE have the ability to promote the electron transfer rate for HZ and PhZ oxidation and have high electrocatalytic activity. Hence, CuNPs(5%)-PANI-Nano-ZSM-5 can be used as a promising electrode material for HZ and PhZ sensing.

The effect of scan rate on the electrochemical oxidation of HZ and PhZ was investigated using CV. Fig. S5, ESI† shows the CVs at CuNPs(5%)-PANI-Nano-ZSM-5/GCE containing HZ and PhZ in 0.1 M PBS (pH 8.5) at various scan rates (10-600 mV/s). The CV results for HZ and PhZ show only an oxidation peak and no reduction peak was observed in the reverse scan which confirms that oxidation of HZ and PhZ is an irreversible electrode process. Further, with increase in the scan rate, the oxidation peak current was increased for both HZ and PhZ. The plot of the oxidation peak current against the square root of scan rate showed a linear relationship indicating a diffusion controlled process. The Semerano coefficient can be calculated from the logarithmic dependence of the electro-oxidation peak current on the scan rate ( $\tan \alpha = \Delta \log I_p / \Delta \log v$ , where  $I_p$  is the oxidation peak current and  $v$  is the scan rate).<sup>41</sup> Plot of the logarithm of anodic peak current vs. logarithm of scan rate provided a straight line with the linear regression equation  $\log I_p = 0.486 \log v + 0.196$  ( $R^2 = 0.995$ ) and  $\log I_p = 0.509 \log v + 0.215$  ( $R^2 = 0.989$ ), for HZ and PhZ, respectively (Fig. S5c-d, ESI†). Slope obtained from the linear behavior between the logarithm of anodic peak current vs. logarithm of scan rate for HZ and PhZ were found to be 0.486 and 0.509, which are close to the theoretical value of 0.5 for a diffusion controlled process. Thus, the electro-catalytic oxidation of HZ and PhZ is mainly dominated by diffusion process.

Chronoamperometry was used to calculate the diffusion coefficient ( $D$ ) and rate constant ( $k$ ) for the electro-catalytic oxidation of HZ and PhZ at CuNPs(5%)-PANI-Nano-ZSM-5/GCE (Fig. S6-S7, ESI† includes experimental details along with a brief discussion). The diffusion coefficients were found to be  $8.4 \times 10^{-6}$  and  $34.8 \times 10^{-6}$  cm<sup>2</sup>/s for HZ and PhZ, respectively. The diffusion coefficient values obtained for HZ and PhZ at CuNPs(5%)-PANI-Nano-ZSM-5/GCE are comparable to recent literature reports.<sup>1, 5, 30</sup> The rate constant values for electro-catalytic oxidation of HZ and PhZ were found as  $9.8 \times 10^4$  and  $1.1 \times 10^4$  1/s M, respectively. This chronoamperometric data indicates that the electrochemical reaction rate for HZ and PhZ at CuNPs(5%)-PANI-Nano-ZSM-5/GCE is fast and the electro-oxidation of HZ and PhZ at CuNPs(5%)-PANI-Nano-ZSM-5/GCE is a typical diffusion controlled process.

The total number of electrons ( $n$ ) involved in the electrochemical oxidation of HZ and PhZ at CuNPs(5%)-PANI-Nano-ZSM-5/GCE can be calculated from the plot of the oxidation peak currents against the square root of scan rate according to the following equation (given below) for a totally irreversible diffusion-controlled process.<sup>30, 50, 51</sup> The total number of electrons

was calculated to be 4.19 and 1.98 for HZ and PhZ, respectively. Hence, a total of 4 and 2 electrons were involved in the electrochemical oxidation of HZ and PhZ, respectively.

$$I_p = 3.01 \times 10^5 n[n_\alpha(1-\alpha)]^{1/2} ACD^{1/2} v^{1/2}$$

Where  $I_p$  is the peak current (A),  $n_\alpha$  is the number of electrons in the rate determining step,  $\alpha$  is charge transfer coefficient,  $A$  is the electrode surface area ( $0.07 \text{ cm}^2$ ),  $C$  is the bulk concentration of analyte ( $\text{mol/cm}^3$ ),  $D$  is the diffusion coefficient of analyte ( $8.4 \times 10^{-6} \text{ cm}^2/\text{s}$  for HZ and  $34.8 \times 10^{-6} \text{ cm}^2/\text{s}$  for PhZ; obtained from the chronoamperometric study), and  $v$  is the scan rate (V/s). The charge transfer coefficient between the analyte (HZ and PhZ) and CuNPs(5%)-PANI-Nano-ZSM-5/GCE was obtained from Tafel plot using the rising part of the current-voltage plot (Fig. S8, ESI†). A slope of  $8.16 \text{ V}^{-1}$  and  $8.35 \text{ V}^{-1}$  was obtained for HZ and PhZ, respectively. Assuming one electron transfer in the rate-determining step ( $n_\alpha = 1$ ), charge transfer coefficient ( $\alpha$ ) was calculated as 0.52 and 0.51 for HZ and PhZ, respectively, according to the equation  $b = n_\alpha(1-\alpha) F/2.3 RT$ , where  $b$  is slope of tafel plot.

The electrochemical oxidation of HZ and PhZ depends on the pH of the buffer solution. Therefore, the electrochemical behavior of HZ and PhZ in phosphate buffer solution with different pH values (4-12) was investigated at CuNPs(5%)-PANI-Nano-ZSM-5/GCE using DPV. The anodic peak current increased with the increase in pH of the medium for both the analytes (Fig. S9, ESI†). HZ exhibited a maximum peak current at pH 8.5 (Fig. S9, ESI†). PhZ exhibited a maximum anodic peak current after pH 5 and remained almost constant between 5 to 8.5 (Fig. S9, ESI†). With further increase in the pH of PBS, the anodic peak current was found to decrease for both the analytes. The  $pK_a$  value for HZ and PhZ are 8.1 and 5.2, respectively.<sup>52, 53</sup> When the pH of PBS is below  $pK_a$ , HZ and PhZ exist in the protonated form. Under the applied positive potential, protonated form of HZ and PhZ are difficult to oxidize, which resulted decrease in their oxidation peak current. When the pH of PBS is higher than  $pK_a$ , the neutral form of the analyte predominates, which resulted high response current. When the pH of PBS is above 9, deprotonation of HZ and PhZ would take place, which is kinetically less favorable, therefore, decrease in the current response was observed.<sup>52, 53</sup> Since the main aim of the study was the simultaneous determination of HZ and PhZ from their binary solution, therefore, pH 8.5 was chosen as an optimum pH value for all the electrochemical experiments.

### 3.4. Individual electro-catalytic oxidation of HZ and PhZ

The individual electro-catalytic oxidation of HZ and PhZ at CuNPs(5%)-PANI-Nano-ZSM-5/GCE was carried out using DPV in 0.1 M PBS (pH 8.5) at a scan rate 20 mV/s (Fig. 6). The DPV results show that both the analytes were oxidized with well-defined and distinguishable sharp oxidation peaks with peak potentials at 402 and 595 mV for PhZ and HZ, respectively, at CuNPs(5%)-PANI-Nano-ZSM-5/GCE (Fig. 6). The peak currents were found to increase linearly with the increase in the concentration of HZ and PhZ in the electrochemical cell. A linear dynamic range from 3 nM to 800  $\mu$ M with a calibration equation of  $I_{\text{PhZ}}(\mu\text{A}) = 5.244 + 0.117 C_{\text{PhZ}}(\mu\text{M})$  ( $R^2 = 0.998$ ) was obtained for PhZ (Fig. 6a, inset). A linear calibration for HZ was found to be in the range of 3 nM to 900  $\mu$ M, with a calibration equation of  $I_{\text{HZ}}(\mu\text{A}) = 10.623 + 0.102 C_{\text{HZ}}(\mu\text{M})$  ( $R^2 = 0.997$ ) (Fig. 6b, inset). These results indicate that CuNPs(5%)-PANI-Nano-ZSM-5/GCE can be used for the individual electrochemical oxidation of HZ and PhZ with significantly high electrocatalytic activity.

### 3.5. Simultaneous electrochemical determination of HZ and PhZ

The main objective of this study is to determine HZ and PhZ simultaneously. DPV was employed for the simultaneous determination of HZ and PhZ at CuNPs(5%)-PANI-Nano-ZSM-5/GCE in 0.1 M PBS (pH 8.5) at a scan rate 20 mV/s (Fig. 7). Fig. 7 shows that two distinguished and sharp anodic peaks at potentials 402 and 595 mV corresponding to the oxidation of PhZ and HZ, respectively, were obtained in the simultaneous determination of PhZ and HZ. These peak potentials match well with their individual anodic peak potentials as discussed in the above section. The voltammograms for the binary mixture were well separated from each other with a potential difference of  $\Delta E_{\text{PhZ-HZ}} = 193$  mV. This peak potential difference is large enough for the simultaneous determination of HZ and PhZ from their binary solution. When the concentration of analytes was increased in the electrochemical cell, a significant increase in the oxidation peak current was observed for both the analytes. The anodic peak current obtained was found to be linearly dependent on the concentration of analytes in the range of 4 nM to 800  $\mu$ M ( $R^2 = 0.998$ ) for HZ and 4 nM to 800  $\mu$ M ( $R^2 = 0.999$ ) for PhZ with the sensitivity of 1.6 and 1.7  $\mu\text{A}/\mu\text{M cm}^2$  and the limit of detection of 1 nM and 1 nM for HZ and PhZ, respectively, (Fig. 7, inset). These results demonstrate that CuNPs(5%)-PANI-Nano-ZSM-5/GCE exhibited excellent electro-catalytic activity toward the simultaneous determination of

HZ and PhZ. Hence, CuNPs(5%)-PANI-Nano-ZSM-5 can be used as an effective candidate for the simultaneous determination of HZ and PhZ. The limit of detection (LOD) was calculated using IUPAC (International Union of Pure and Applied Chemistry) definitions, using the standard approach of alternative (SA).<sup>54</sup>

$$\text{LOD}_{\text{SA}} = 3S_b/q$$

Where  $S_b$  is the standard deviation of the blank signal, and  $q$  is the slope of the calibration curve.

A comparison for the electrochemical oxidation of HZ and PhZ at copper nanoparticles decorated PANI-Nano-ZSM-5 nanocomposite modified GCE with different weight ratio is provided in Fig. S10, ESI†. It may be noted that with increase in the amount of CuNPs on PANI-Nano-ZSM-5 support, the electrochemical activity was increased. This shows that higher loading of CuNPs in nanocomposite material is better for the high electrocatalytic activity. However, with further increase in CuNPs content (after CuNPs(5%)), the electro-catalytic activity was not increased (Fig. S10, ESI†). The electrocatalytic activity of CuNPs(10%)-PANI-Nano-ZSM-5/GCE was found to be low when compared to CuNPs(5%)-PANI-Nano-ZSM-5/GCE. These results clearly show that the highly dispersed CuNPs on the surface of PANI-Nano-ZSM-5 enhances the accessibility of analytes to the active sites and improved the catalytic activity of nanocomposite material. Therefore, CuNPs(5%)-PANI-Nano-ZSM-5/GCE was chosen for the electrochemical oxidation of HZ and PhZ. DPV was further used to investigate the electrocatalytic activity of CuNPs(5%)-PANI/GCE, CuNPs(5%)-Nano-ZSM-5/GCE, PANI/GCE, Nano-ZSM-5/GCE, and bare GCE in the simultaneous determination of HZ and PhZ. However, in this manuscript only a comparative data is presented. A comparison of CuNPs(5%)-PANI-Nano-ZSM-5/GCE with other modified electrodes and bare GCE in the simultaneous determination of HZ and PhZ is shown in (Fig. 8 and Fig. S11, ESI†). Bare GCE exhibited a broad oxidation peak in the simultaneous determination of HZ and PhZ (Fig. S11, ESI†). Hence, bare GCE was unable to distinguish between HZ and PhZ and cannot be applied in the simultaneous determination of HZ and PhZ. Fig. S11, ESI† shows that Nano-ZSM-5/GCE and PANI/GCE also exhibited somewhat broad oxidation peaks for HZ and PhZ at higher potential with a low current response when compared to CuNPs(5%)-PANI-Nano-ZSM-5/GCE. This further confirms that Cu nanoparticles play an important role in the electrochemical oxidation of HZ and PhZ and have an electrocatalytic effect on the oxidation of HZ and PhZ.

CuNPs(5%)-Nano-ZSM-5/GCE and CuNPs(5%)-PANI/GCE also exhibited sharp and distinguishable oxidation peaks for the simultaneous determination of HZ and PhZ but with a very low current response when compared to CuNPs(5%)-PANI-Nano-ZSM-5/GCE. The DPV results clearly show that CuNPs(5%)-PANI-Nano-ZSM-5/GCE exhibited the highest electrocatalytic activity and sensitivity toward the simultaneous determination of HZ and PhZ among the various modified electrodes investigated in this study and bare GCE (Fig. 8 and Fig. S11, ESI<sup>†</sup>). These observations provide evidence that PANI coated Nano-ZSM-5 nanocomposite material is more active than bulk PANI or Nano-ZSM-5. The remarkable high activity of CuNPs(5%)-PANI-Nano-ZSM-5/GCE can be attributed to the synergistic contribution provided by highly dispersed CuNPs, conductive PANI and high surface area Nano-ZSM-5. Moreover, PANI film at Nano-ZSM-5 favors the facile transportation of electrons through the PANI-Nano-ZSM-5 matrix. The inter-crystalline mesoporosity in Nano-ZSM-5 provides an efficient transport path for reactant/product molecules because of the short diffusion length and mesoporosity. The comparison of results shown in this paper with literature reports is provided in Table S1, ESI<sup>†</sup>. It is clear from Table S1, ESI<sup>†</sup> that the present sensor is able to detect HZ and PhZ simultaneously with a wide linear range and low limit of detection when compared to literature reports. High sensitivity, fast response, wide linear range, and low limit of detection made CuNPs(5%)-PANI-Nano-ZSM-5 nanocomposite as an effective electrochemical sensor for HZ and PhZ.

The abundant surface silanol groups present in Nano-ZSM-5 and -NH group present in polyaniline would interact well with the amine group of HZ and PhZ due to hydrogen bonding. Furthermore, the porous nature of Nano-ZSM-5 is favorable for the diffusion of analyte to the electrode surface. During the anodic scan, PhZ and HZ are electrochemically oxidized around 434 mV and 689 mV at PANI-Nano-ZSM-5/GCE, Nano-ZSM-5/GCE, and PANI/GCE. These results indicate that Nano-ZSM-5 and PANI promote the oxidation of HZ and PhZ due to the favorable interaction between the modified electrode surface and analytes (HZ and PhZ). The electrochemical oxidation behavior of HZ and PhZ was further improved in the presence of CuNPs. The higher current response and decrease in the oxidation peak potential in the electrochemical oxidation of HZ and PhZ at CuNPs(5%)-PANI-Nano-ZSM-5/GCE are indicative of the catalytic effect provided by CuNPs. Based on the results obtained in this study and the literature reports, the mechanism for the electrochemical oxidation of HZ and PhZ at CuNPs(5%)-PANI-Nano-ZSM-5/GCE is proposed.<sup>4, 55-57</sup>

The electrochemical oxidation of PhZ and HZ was observed at anodic peak potentials 402 and 595 mV, respectively, at CuNPs(5%)-PANI-Nano-ZSM-5/GCE with the high current response. The oxidation of HZ and PhZ occurs in the potential range of 0.4 to 0.6 V, where the oxidation of Cu(II) to Cu(III) occurred (Fig. 4).<sup>32, 48</sup> Cu(II) is electrochemically oxidized to strong oxidizing Cu(III) species at the electrode surface (peak iii) (Fig. 4). Cu(III) then oxidizes the analytes (HZ and PhZ) and regenerates reduced form of Cu(II) (Scheme 1). In this study, electrochemically generated Cu(III) acts as oxidizing agent and analytes act as reducing agent to regenerate Cu(II). Therefore, one may conclude that Cu(III) species act as an electron transfer mediator in the electrochemical oxidation of HZ and PhZ at CuNPs(5%)-PANI-Nano-ZSM-5/GCE. It may be noted that Cu(II) as redox mediator present in the electrochemical cell along with analytes is not suitable for the catalytic electrochemical oxidation of HZ and PhZ (Fig. S12, ESI†). In order to see the influence of redox mediator (simply added in the electrochemical cell), the DPV was performed at PANI-Nano-ZSM-5/GCE, Nano-ZSM-5/GCE, and PANI/GCE in the presence of 50  $\mu$ M/1 mM/2 mM/5 mM CuCl<sub>2</sub> (different concentrations of CuCl<sub>2</sub>) added in the electrochemical cell along with the analytes (HZ and PhZ). The current response for the oxidation of HZ and PhZ was not increased at PANI-Nano-ZSM-5/GCE, Nano-ZSM-5/GCE, and PANI/GCE in the presence of Cu(II) in the electrochemical cell when compared with PANI-Nano-ZSM-5/GCE, Nano-ZSM-5/GCE, and PANI/GCE in the absence of Cu(II) (Fig. S12, ESI†). It may be noted that the current response in the presence of 50  $\mu$ M/1 mM/2 mM/5 mM CuCl<sub>2</sub> was almost similar. These results confirm that Cu(II) present in the electrochemical cell is unable to catalyze the oxidation of analytes HZ and PhZ. Since the electron transfer takes place at the electrode surface only, Cu(II) is required to reach the electrode surface first so that it can be electrochemically oxidized to strongly oxidizing Cu(III), which is responsible for the oxidation of HZ and PhZ. It may be noted that potential is applied in the positive direction during the anodic scan. Therefore, the positively charged Cu(II) would experience a repulsive force with the electrode surface during the anodic scan and would be repelled by the electrode surface. Thus, Cu(II) present in the electrochemical cell along with analytes is not suitable for the catalytic electrochemical oxidation of HZ and PhZ.

### 3.6. Reproducibility, stability, and anti-interference property of the sensor

The reproducibility and stability of the developed sensor were evaluated in the sensing studies. Five, CuNPs(5%)-PANI-Nano-ZSM-5/GCE were constructed and their current response to 1  $\mu\text{M}$  concentration of HZ and PhZ was investigated (Fig. S13, ESI<sup>†</sup>). The relative standard deviation (RSD) was found to be 2.3 % and 2.1 % for HZ and PhZ, respectively confirming that the fabrication method was highly reproducible. The stability of CuNPs(5%)-PANI-Nano-ZSM-5/GCE was examined by recording repetitive CVs for 50 scans in PBS (pH 8.5) at a scan rate 50 mV/s in the presence of HZ and PhZ. No obvious change in the peak current was observed after 50 cycles, which confirms that CuNPs(5%)-PANI-Nano-ZSM-5/GCE is highly stable. The long term stability of the sensor was evaluated by measuring its sensitivity toward 1  $\mu\text{M}$  concentration of HZ and PhZ for 20 days (Fig. S14, ESI<sup>†</sup>). The sensor was stored in the refrigerator at 278 K and its sensitivity was tested at the interval of 5 days. Prior to each measurement, electrode was washed with 0.1 M PBS and repetitive CV were run in blank 0.1 M PBS (pH 8.5). The results confirmed that the DPV response of the electrode to the same concentration of HZ and PhZ remained almost same with RSD 3.1 % and 2.8 % for HZ and PhZ respectively, indicating that the modified electrode has excellent stability. In order to investigate the selectivity of CuNPs(5%)-PANI-Nano-ZSM-5/GCE toward simultaneous determination of HZ and PhZ; DPV measurements were performed in the presence of various interfering agents. The possible interferences of some inorganic ions and organic compounds were investigated by adding a suitable concentration of additive in binary mixture solution containing 1  $\mu\text{M}$  of HZ and PhZ. The results showed that 120 fold excess of  $\text{K}^+/\text{Na}^+/\text{Cl}^-/\text{HPO}_4^{2-}/\text{H}_2\text{PO}_4^-/\text{Ca}^{2+}/\text{Mn}^{2+}/\text{Fe}^{3+}/\text{Cu}^{2+}/\text{Zn}^{2+}/\text{Mg}^{2+}$  had no effect on the peak currents for the oxidation of HZ and PhZ. The presence of other common interferents (50 fold) such as nitrite, nitrate, ammonia, 2,4-dinitroaniline, 2,4-dinitrophenylhydrazine, aniline, diphenylamine, aminophenol isomers, dihydroxybenzene isomers, and phenol did not show any change in the peak current response confirming that no interference for these common species occurred.

### 3.7. Determination of HZ and PhZ in water samples

In order to show the practical application of the developed sensor; experiments were performed to determine the concentration of HZ and PhZ in tap water and river water samples and the results are summarized in Table 2. The values of recovery were in the range from 99 to 101 %,

suggesting the accuracy of CuNPs(5%)-PANI-Nano-ZSM-5/GCE based sensor. These results confirm that proposed sensor is reliable and sensitive enough for the determination of HZ and PhZ in different real water bodies and can be employed for the routine determination of HZ and PhZ.

#### 4. Conclusions

In summary, copper nanoparticles decorated polyaniline-zeolite nanocomposite materials were synthesized. Transmission electron microscopy investigations confirmed that highly dispersed copper nanoparticles were supported on polyaniline-zeolite nanocomposite. SEM/TEM also confirmed that polyaniline film was formed on the surface of Nano-ZSM-5 and no separate polyaniline phase was formed. An electrochemical sensor based on copper nanoparticles decorated PANI-Nano-ZSM-5 modified glassy carbon electrode was fabricated for the simultaneous determination of environmental pollutants hydrazine and phenylhydrazine. The results demonstrated that the developed sensor exhibited high electro-catalytic activity, sensitivity, and stability in hydrazine and phenylhydrazine detection. The high activity of CuNPs(5%)-PANI-Nano-ZSM-5 can be attributed to the synergistic contribution provided by highly dispersed Cu nanoparticles and conductive PANI film at high surface area Nano-ZSM-5. The analytical performance of the developed sensor was extended in the determination of these pollutants in different water bodies with satisfactory results. The proposed methodology is simple, rapid and provides a potentially new analytical platform for the detection of hydrazine and phenylhydrazine. Further, the application of CuNPs-PANI-Nano-ZSM-5 nanocomposite material can be extended in hydrazine fuel cells.

#### Acknowledgements

Authors thank Department of Science and Technology, New Delhi for financial assistance (DST grant SB/S1/PC-91/2012). BK is grateful to CSIR, New Delhi for SRF fellowship. Authors are also thankful to Director IIT Ropar for constant encouragement.

#### Supporting Information

Electronic Supplementary Information (ESI) available. See DOI:

## References

1. H. R. Zare, Z. Shekari, N. Nasirizadeh and A. A. Jafari, *Catal. Sci. Tech.*, 2012, **2**, 2492.
2. J. Ding, S. Zhu, T. Zhu, W. Sun, Q. Li, G. Wei and Z. Su, *RSC Adv.*, 2015, **5**, 22935.
3. A. A. Ibrahim, G. Dar, S. A. Zaidi, A. Umar, M. Abaker, H. Bouzid and S. Baskoutas, *Talanta*, 2012, **93**, 257.
4. S. B. Khan, M. Faisal, M. M. Rahman, I. Abdel-Latif, A. A. Ismail, K. Akhtar, A. Al-Hajry, A. M. Asiri and K. A. Alamry, *New J. Chem.*, 2013, **37**, 1098.
5. F. Gholamian, M. A. Sheikh-Mohseni and H. Naeimi, *Mat. Sci. Eng. C*, 2012, **32**, 2344.
6. S. Tafazoli, M. Mashregi and P. J. O'Brien, *Toxicol. Appl. Pharmacol.*, 2008, **229**, 94.
7. S. Garrod, M. E. Bollard, A. W. Nicholls, S. C. Connor, J. Connelly, J. K. Nicholson and E. Holmes, *Chem. Res. Toxicol.*, 2005, **18**, 115.
8. G. Choudhary and H. Hansen, *Chemosphere*, 1998, **37**, 801.
9. N. Rastakhiz, A. Kariminik, V. Soltani-Nejad and S. Roodsaz, *Int. J. Electrochem. Sci.*, 2010, **5**, 1203.
10. A. Safavi and M. A. Karimi, *Talanta*, 2002, **58**, 785.
11. M. Mori, K. Tanaka, Q. Xu, M. Ikedo, H. Taoda and W. Hu, *J. Chromatogr. A*, 2004, **1039**, 135.
12. Q. Yi and W. Yu, *J. Electroanal. Chem.*, 2009, **633**, 159.
13. M. George, K. S. Nagaraja and N. Balasubramanian, *Talanta*, 2008, **75**, 27.
14. M. Arab Chamjangali, G. Bagherian and S. Ameri, *J. Hazard. Mater.*, 2009, **166**, 701.
15. W. Siangproh, O. Chailapakul, R. Laocharoensuk and J. Wang, *Talanta*, 2005, **67**, 903.
16. M. Mazloum-Ardakani, Z. Taleat, H. Beitollahi and H. Naeimi, *Nanoscale*, 2011, **3**, 1683.
17. Y. He, J. Zheng and S. Dong, *Analyst*, 2012, **137**, 4841.
18. H. Wang, Y. Ma, R. Wang, J. Key, V. Linkov and S. Ji, *Chem. Commun.*, 2015, **51**, 3570.
19. J. Zhang, W. Gao, M. Dou, F. Wang, J. Liu, Z. Li and J. Ji, *Analyst*, 2015, **140**, 1686.
20. H. Wang, X. Bo, J. Ju and L. Guo, *Catal. Sci. Tech.*, 2012, **2**, 2327.
21. C. Batchelor-McAuley, C. E. Banks, A. O. Simm, T. G. Jones and R. G. Compton, *Analyst*, 2006, **131**, 106.
22. C. Tan, X. Xu, F. Wang, Z. Li, J. Liu and J. Ji, *Sci. China Chem.*, 2013, **56**, 911.

23. B. Šljukić, C. E. Banks, A. Crossley and R. G. Compton, *Electroanalysis*, 2006, **18**, 1757.
24. S. Shukla, S. Chaudhary, A. Umar, G. R. Chaudhary and S. K. Mehta, *Sens. Actuators, B: Chem.*, 2014, **196**, 231.
25. J. Lei, X. Lu, W. Wang, X. Bian, Y. Xue, C. Wang and L. Li, *RSC Adv.*, 2012, **2**, 2541.
26. K. NamáHan, C. AiáLi, M.-P. NgocáBui and G. HunáSeong, *Chem. Commun.*, 2011, **47**, 938.
27. X. Luo, J. Pan, K. Pan, Y. Yu, A. Zhong, S. Wei, J. Li, J. Shi and X. Li, *J. Electroanal. Chem.*, 2015, **745**, 80.
28. A. J. Jeevagan and S. A. John, *RSC Adv.*, 2013, **3**, 2256.
29. A. Umar, M. M. Rahman, S. H. Kim and Y.-B. Hahn, *Chem. Commun.*, 2008, 166.
30. M. U. Anu Prathap, V. Anuraj, B. Satpati and R. Srivastava, *J. Hazard. Mater.*, 2013, **262**, 766.
31. R. Ojani, J.-B. Raouf and S. Zamani, *Appl. Surf. Sci.*, 2013, **271**, 98.
32. B. Kaur, M. U. Anu Prathap and R. Srivastava, *ChemPlusChem*, 2012, **77**, 1119.
33. B. Kaur, B. Satpati and R. Srivastava, *New J. Chem.*, 2015, **39**, 1115.
34. B. Kaur and R. Srivastava, *Electrochim. Acta*, 2014, **133**, 428.
35. B. Kaur and R. Srivastava, *Electroanalysis*, 2014, **26**, 1078.
36. B. Kaur and R. Srivastava, *Colloids Surf., B*, 2014, **118**, 179.
37. B. Kaur and R. Srivastava, *Electroanalysis*, 2014, **26**, 1739.
38. B. Kaur and R. Srivastava, *J. Nanosci. Nanotechnol.*, 2014, **14**, 6539.
39. B. Kaur and R. Srivastava, *Electrochim. Acta*, 2014, **141**, 61.
40. B. Kaur, R. Srivastava and B. Satpati, *New J. Chem.*, 2015, DOI: 10.1039/C4NJ02369B.
41. B. Kaur and R. Srivastava, *Sens. Actuators, B: Chem.*, 2015, **211**, 476.
42. M. U. Anu Prathap, B. Thakur, S. N. Sawant and R. Srivastava, *Colloids Surf., B*, 2012, **89**, 108.
43. M. Shi, H. S. Kwon, Z. Peng, A. Elder and H. Yang, *ACS Nano*, 2012, **6**, 2157.
44. K. Cheirmadurai, S. Biswas, R. Murali and P. Thanikaivelan, *RSC Adv.*, 2014, **4**, 19507.
45. M. U. Anu Prathap, B. Kaur and R. Srivastava, *J. Colloid Interface Sci.*, 2012, **381**, 143.
46. P. Alexandridis and T. A. Hatton, *Colloids Surf., A*, 1995, **96**, 1.

47. S. Xuan, Y.-X. J. Wang, K. C.-F. Leung and K. Shu, *J. Phys. Chem. C*, 2008, **112**, 18804.
48. J. M. Marioli and T. Kuwana, *Electrochim. Acta*, 1992, **37**, 1187.
49. G. Brisard, J. Rudnicki, F. McLarnon and E. Cairns, *Electrochim. Acta*, 1995, **40**, 859.
50. H. R. Zare and N. Nasirizadeh, *Electrochim. Acta*, 2007, **52**, 4153.
51. H. Zare, N. Nasirizadeh and M. M. Ardakani, *J. Electroanal. Chem.*, 2005, **577**, 25.
52. G. Wang, C. Zhang, X. He, Z. Li, X. Zhang, L. Wang and B. Fang, *Electrochim. Acta*, 2010, **55**, 7204.
53. Y. Liu, Y. Li and X. He, *Anal. Chim. Acta*, 2014, **819**, 26.
54. J. Mocak, A. M. Bond, S. Mitchell and G. Scollary, *Pure Appl. Chem.*, 1997, **69**, 297.
55. M. R. Majidi, A. Jouyban and K. Asadpour-Zeynali, *Electrochim. Acta*, 2007, **52**, 6248.
56. Y.-Y. Tang, C.-L. Kao and P.-Y. Chen, *Anal. Chim. Acta*, 2012, **711**, 32.
57. X. Yan, F. Meng, S. Cui, J. Liu, J. Gu and Z. Zou, *J. Electroanal. Chem.*, 2011, **661**, 44.

**Figures, Tables and Scheme captions****Figures**

- Fig. 1 (a) XRD patterns of PANI, Nano-ZSM-5, PANI-Nano-ZSM-5, and CuNPs(5%)-PANI-Nano-ZSM-5; and (b) N<sub>2</sub>-adsorption isotherms of PANI, Nano-ZSM-5, and PANI-Nano-ZSM-5 materials..
- Fig. 2 (a) Low magnification TEM images, (b-c) High magnification TEM image showing copper nanoparticles decorated on PANI-Nano-ZSM-5 surface, (d) HRTEM image showing copper nanoparticles for CuNPs(5%)-PANI-Nano-ZSM-5 nanocomposite.
- Fig. 3 (a) STEM-HAADF image of CuNPs(5%)-PANI-Nano-ZSM-5 nanocomposite, (b) EDX spectra from a rectangular region marked by area 1 in (a).
- Fig. 4 CV response of CuNPs(5%)-PANI-Nano-ZSM-5/GCE in 0.1 M PBS (pH 8.5) at a scan rate of 50 mV/s.
- Fig. 5 Comparison of CVs in a 0.1 M PBS (pH 8.5) containing (a,b) PhZ (10 μM) and (c,d) HZ (10 μM) at CuNPs(5%)-PANI-Nano-ZSM-5/GCE and bare GCE at a scan rate of 50 mV/s.
- Fig. 6 DPVs at CuNPs(5%)-PANI-Nano-ZSM-5/GCE in 0.1 M PBS (pH 8.5) by varying the concentrations of (a) PhZ and (b) HZ. DPV parameters were selected as: pulse amplitude: 50 mV, pulse width: 50 ms, scan rate: 20 mV/s. Inset shows the calibration plot.
- Fig. 7 DPVs of the binary mixture containing varying concentrations of HZ and PhZ at CuNPs(5%)-PANI-Nano-ZSM-5/GCE in 0.1 M PBS (pH 8.5). DPV parameters were selected as: pulse amplitude: 50 mV, pulse width: 50 ms, scan rate: 20 mV/s. Inset shows the calibration plot for HZ and PhZ.
- Fig. 8 Comparison of the sensitivity for HZ and PhZ electro-oxidation at different modified glassy carbon electrodes investigated in this study.

**Table**

Table 1 Physico-chemical characteristics of various materials investigated in this study.

Table 2 Determination of HZ and PhZ in different water bodies at CuNPs(5%)-PANI-Nano-ZSM-5/GCE.

**Scheme**

Scheme 1 Electrochemical oxidation of HZ and PhZ at CuNPs(5%)-PANI-Nano-ZSM-5/GCE.

**Table 1**

<b>S.No.</b>	<b>Sample</b>	<b>Total surface area <math>S_{\text{BET}}</math> (m<sup>2</sup>/g)</b>	<b>External surface area (m<sup>2</sup>/g)</b>	<b>Total pore volume (cm<sup>3</sup>/g)</b>
<b>1.</b>	Nano-ZSM-5	548	365	0.58
<b>2.</b>	PANI	45	-	0.03
<b>3.</b>	PANI-Nano-ZSM-5	297	123	0.41

**Table 2**

<b>Sample</b>	<b>Analyte</b>	<b>Taken (nM)</b>	<b>Spiked (nM)</b>	<b>Found<sup>a</sup> (nM)</b>	<b>Recovery (%)</b>
Tap Water	PhZ	-	500	501	100.2
	HZ	-	500	498	99.6
Artificial tap water sample containing known amounts of analytes	PhZ	300	-	299	99.6
	PhZ	300	500	802	100.6
	HZ	300	-	301	100.3
	HZ	300	500	803	101.0
Sutlej river water (Rupnagar, Punjab, India)	PhZ	-	500	497	99.4
	HZ	-	500	502	100.4

<sup>a</sup>Average value of five determinations.

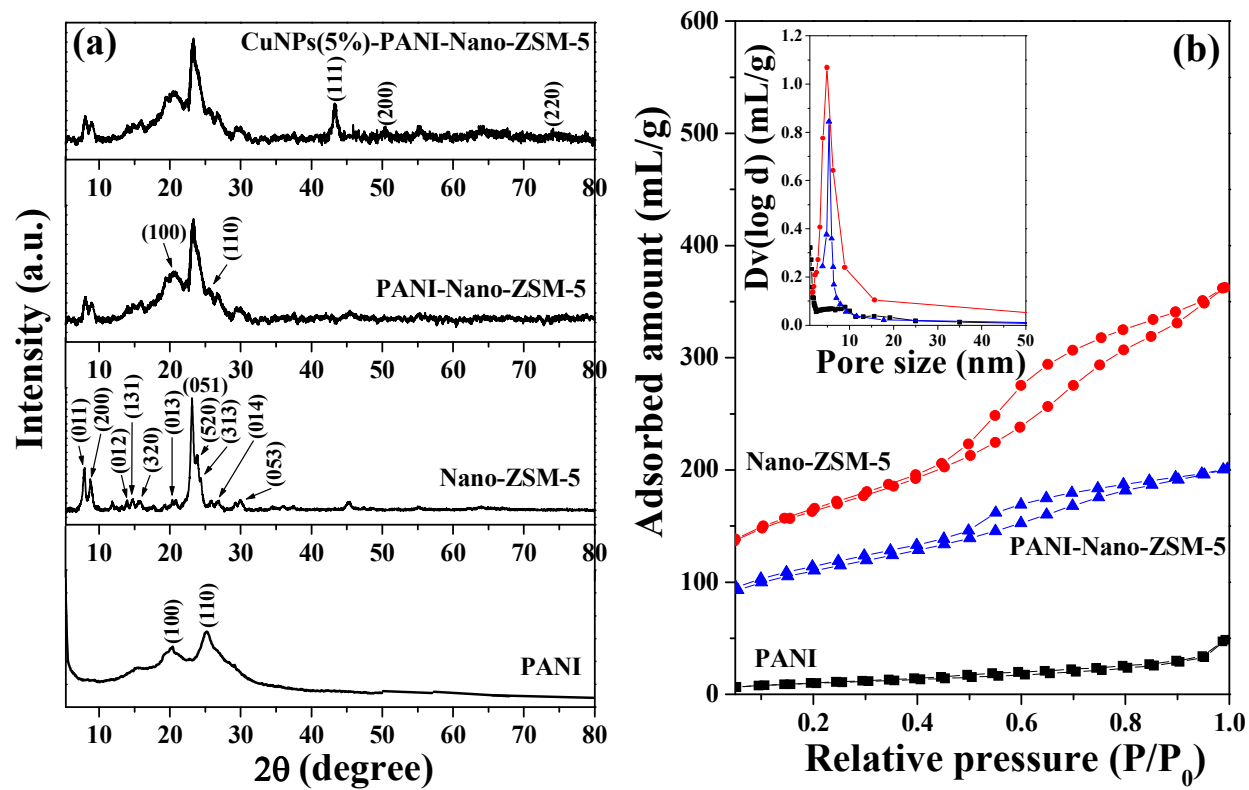


Fig. 1

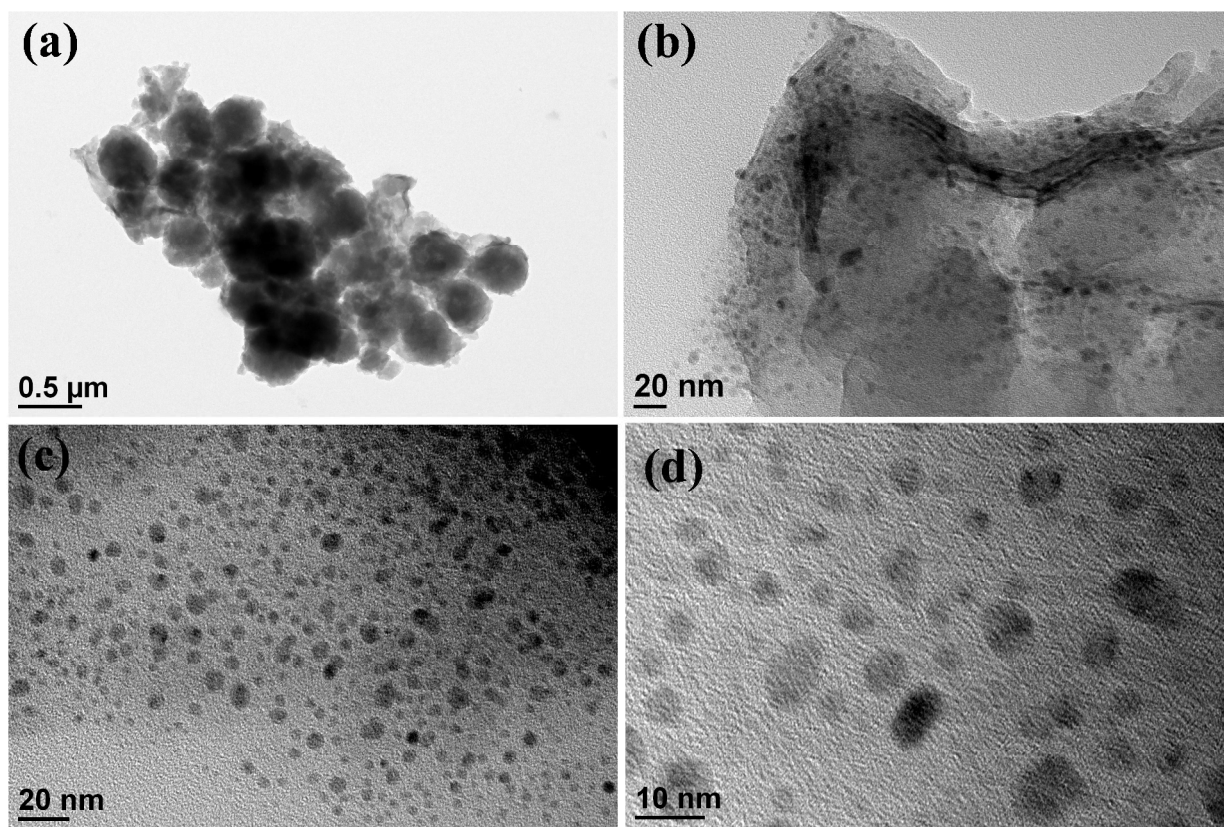


Fig. 2

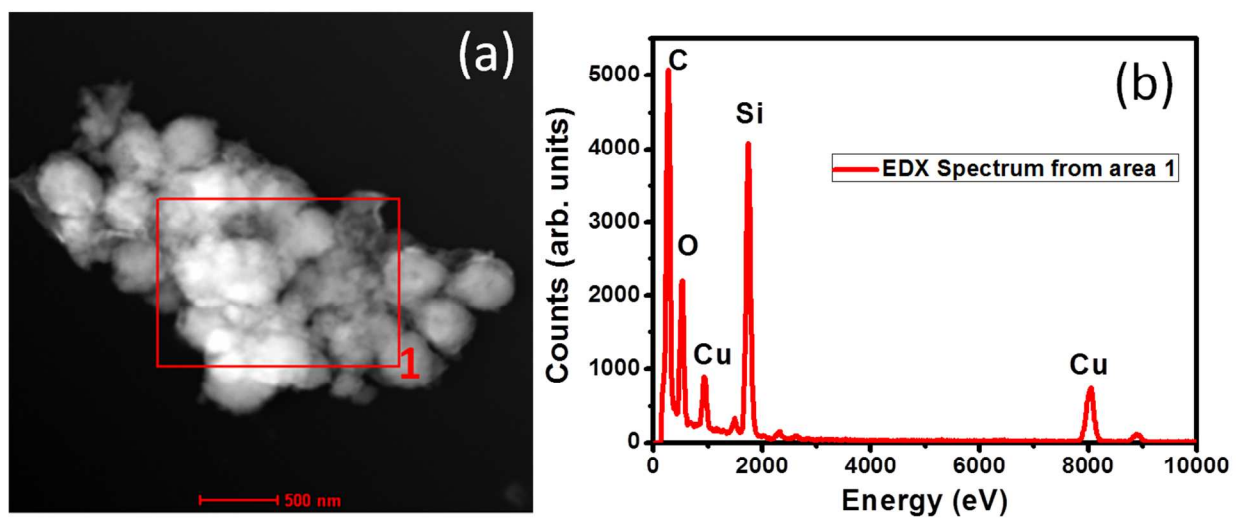


Fig. 3

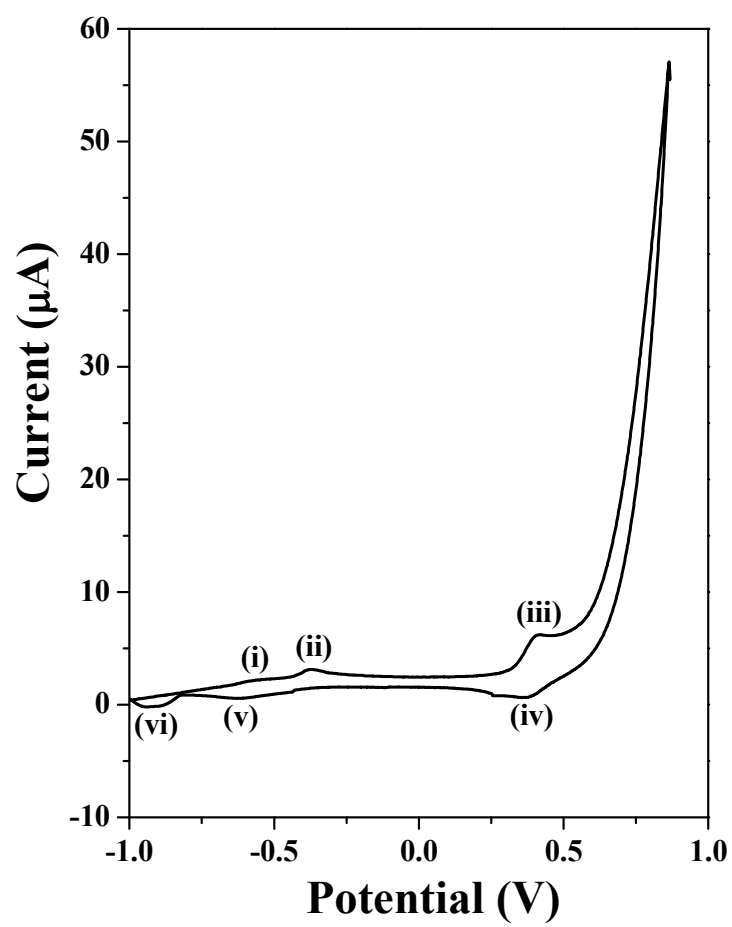


Fig. 4

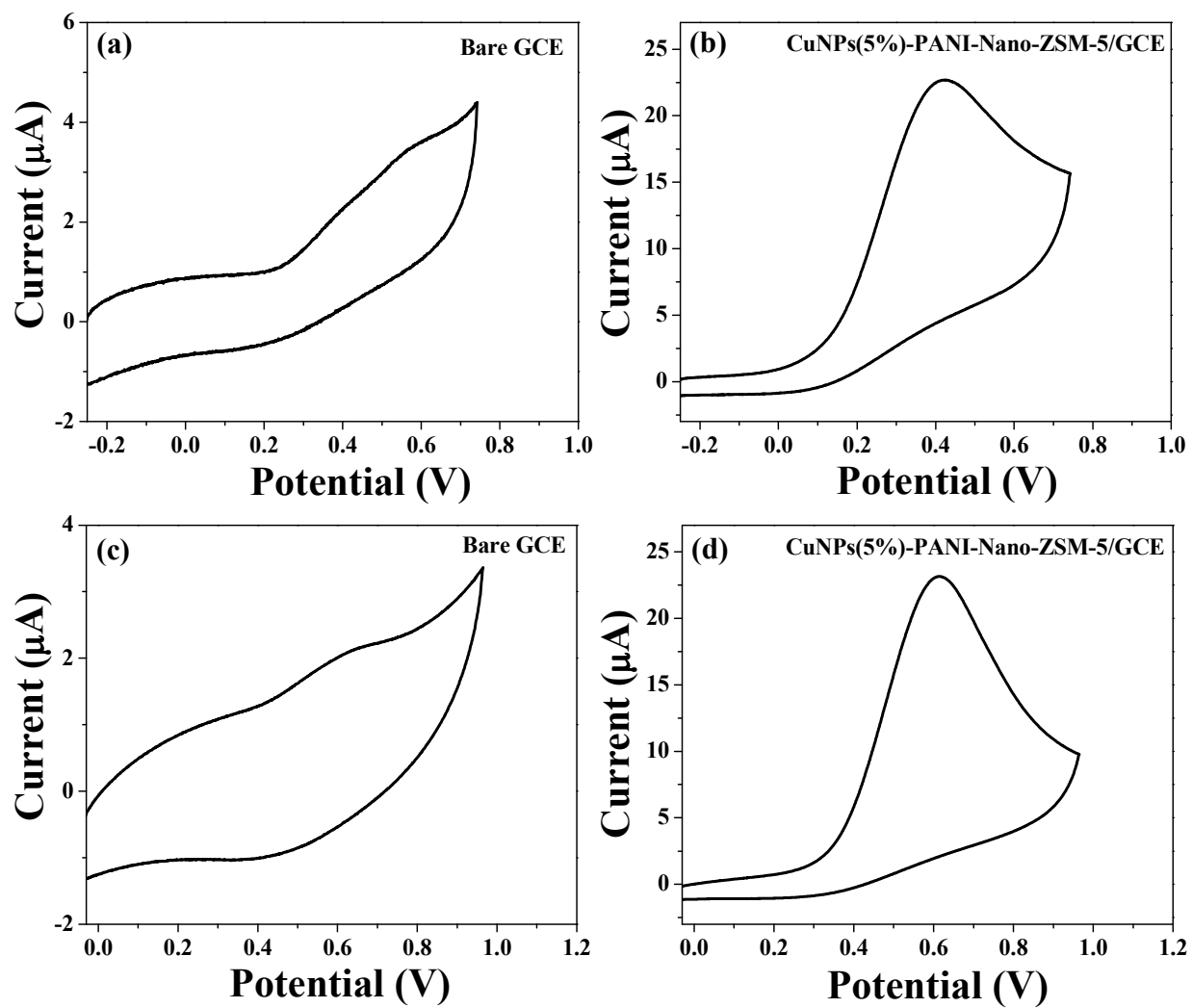


Fig. 5

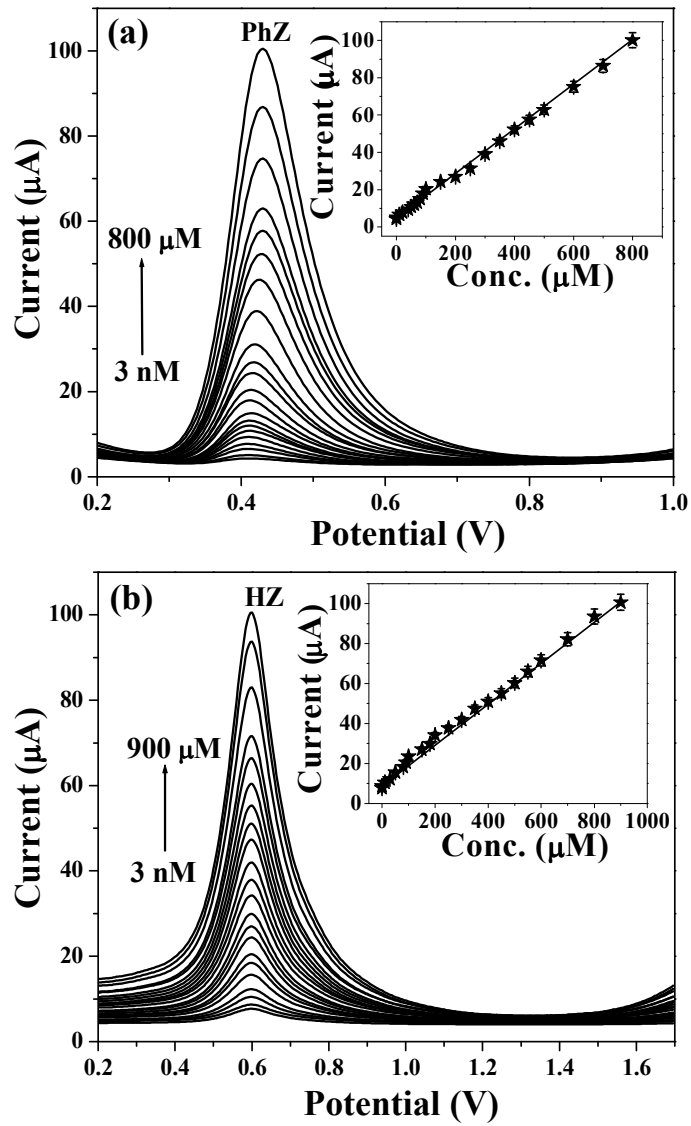


Fig. 6

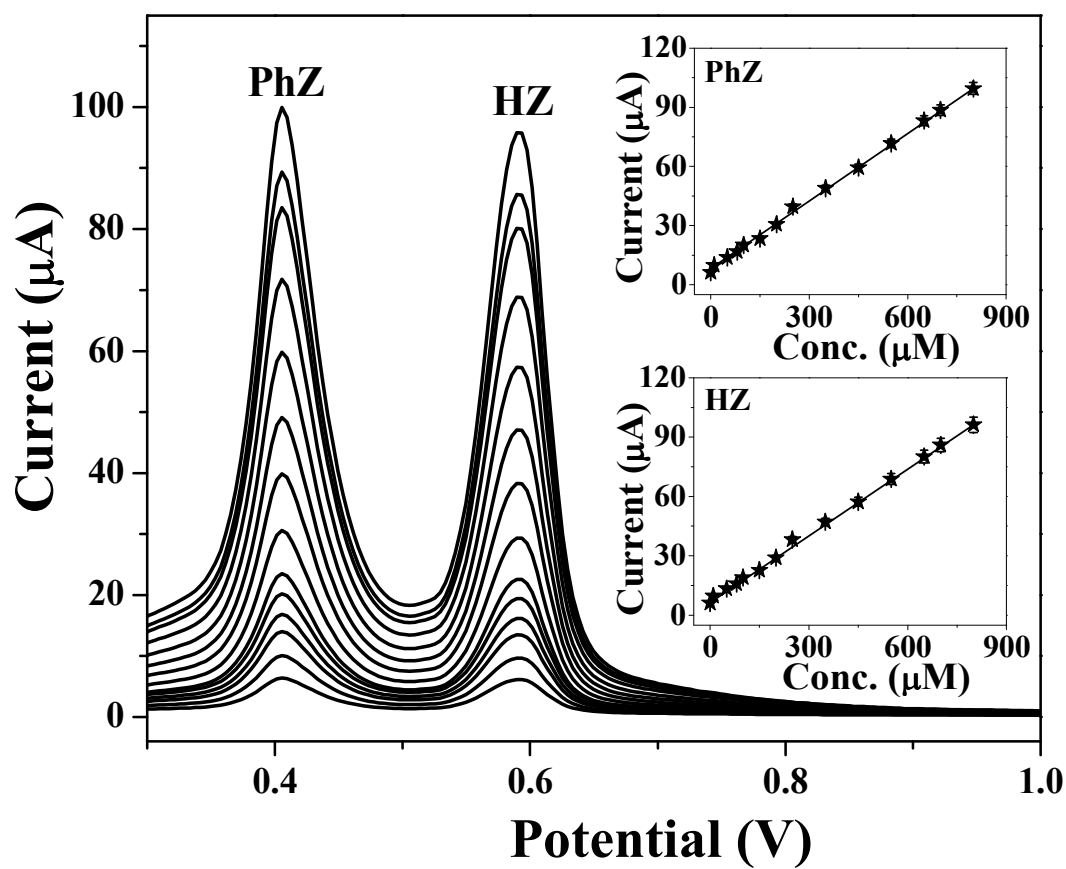


Fig. 7

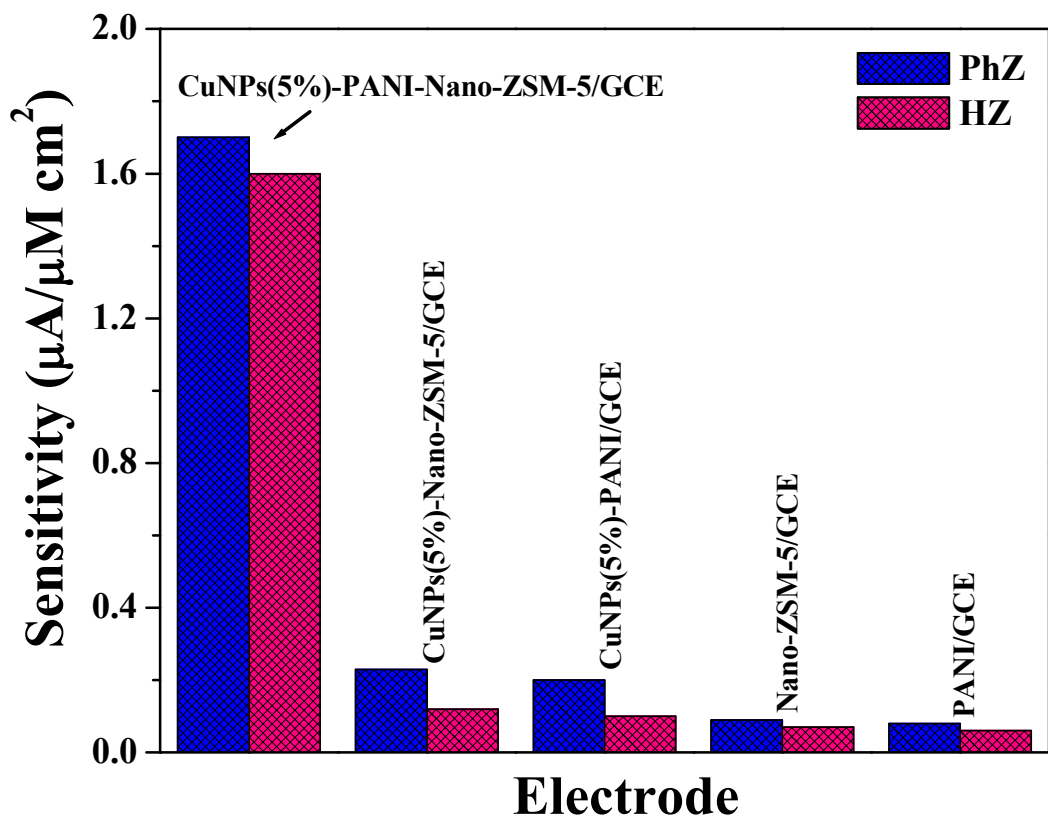
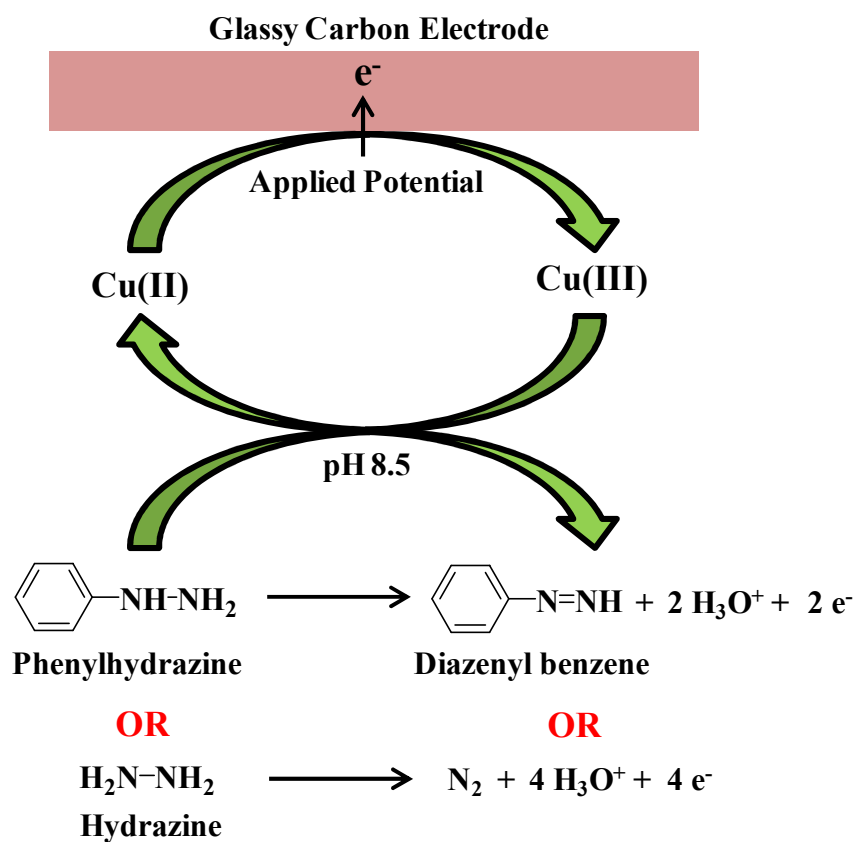
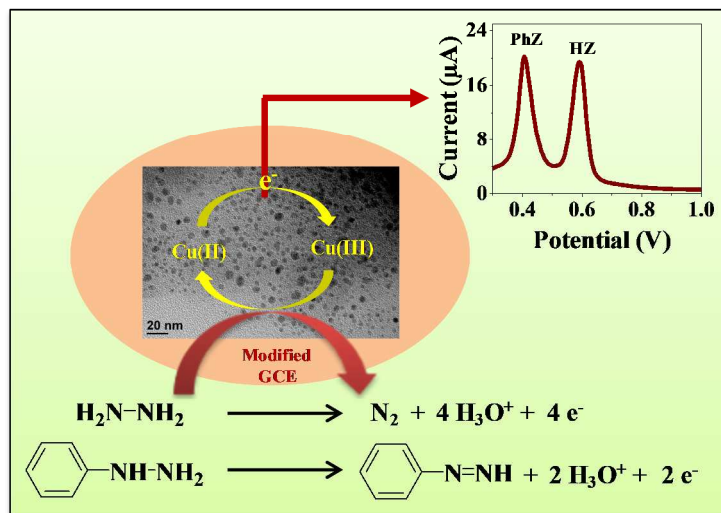


Fig. 8



Scheme 1

### Graphical Abstract



The high electrocatalytic activity of CuNPs-PANI-Nano-ZSM-5 nanocomposite can be attributed to the synergistic contribution provided by highly dispersed copper nanoparticles and conductive PANI film at high surface area Nano-ZSM-5.